# Apatite as an Indicator of Pge Mineralization Formation as Exemplified by Anorthosites of the Kievey Deposit, Fedorova-Pana Layered Complex, Kola Peninsula

Artyom Sushchenko , Nikolay Groshev * , Tatyana Rundkvist , Alena Kompanchenko , Yevgeny Savchenko

Posted Date: 2 November 2023

doi: 10.20944/preprints202311.0074.v1

Keywords: apatite; disseminated sulfides; platinum group elements; layered intrusions; Fedorova-Pana Complex; Kola Peninsula

*Article*

# Apatite as an Indicator of PGE Mineralization Formation as Exemplified by Anorthosites of the Kievey Deposit, Fedo-Rova-Pana Layered Complex, Kola Peninsula

**Artyom Sushchenko, Nikolay Groshev *, Tatyana Rundkvist, Alena Kompanchenko and Yevgeny Savchenko**

Geological Institute, Kola Science Center, Russian Academy of Sciences (GI KSC RAS), Apatity 184209, Russia; a.sushchenko@ksc.ru (A.S.), t.rundkvist@ksc.ru (T.R.), a.kompanchenko@ksc.ru (A.K.), ye.savchenko@ksc.ru (Ye.S.)
* Correspondence: n.groshev@ksc.ru (N.G.); Tel.: +7-815-55-79376

**Abstract:** This paper presents petrography, EDS, LA-ICP-MS, and Raman spectroscopy data characterizing mineral associations and composition of apatite group minerals from anorthosites of the Kievey deposit, North PGE Reef, Fedorova-Pana Complex, Russia. The mineralized coarse-grained anorthosite belongs to the most common rock type of the main ore body and hosts irregular interstitial sulfide dissemination of 5–7 vol. %. Apatite in the anorthosite forms a) euhedral grains included in the marginal parts of cumulus plagioclase laths, and b) xenomorphic grains associated with intercumulus minerals. The composition of apatite evolves along a narrow trend from fluorapatite to hydroxylapatite. The F content in apatite reaches 2.21 wt. %; the maximum Sr and REE concentration is 257 and 5623 ppm respectively, while the average ratio of $La/Yb_N$=11.78, Sr/Sr*=0.01, and Eu/Eu*=0.06. Compared to classic PGE reefs in layered intrusions such as Bushveld in South Africa and Stillwater in the United States, the mineralized anorthosite is distinguished by apatite with an unusual low chlorine concentration of only 0.46 wt. %. One of suggested reason of this difference is percolating nature of sulfide liquid which has not been enriched in PGE in situ.

**Keywords:** apatite; disseminated sulfides; platinum group elements; layered intrusions; Fedorova-Pana Complex; Kola Peninsula

## 1. Introduction

Apatite is a common accessory mineral in mafic-ultramafic complexes. According to many researchers a composition of apatite can be used as an indicator of mineral- and ore-forming processes. Boudreau with colleagues [1] suggested that the presence of chlorapatite reflects the saturation of the magmatic fluid with chlorine and is an important indicator for genesis of platinum group elements (PGE) mineralization in layered mafic-ultramafic rocks. Thereafter Boudreau [2], developing the assumption of the importance of chlorine in the transport of PGE, compared the composition of apatite from intrusions of the Yilgarn block (Western Australia) and the Duluth Complex (Minnesota, USA) with that from the Bushveld (South Africa) and Stillwater complexes (Montana, USA). The result showed that the geochemistry of apatite and other halogen-bearing minerals can be a useful guide to assessing PGE potential of layered intrusions. It is assumed that chlorine in complex compounds is involved in transport and concentration of PGE, especially in the case of high-grade thin and very continuous layers known as PGE reefs.

In recent years, many researchers of mafic-ultramafic ore-bearing rocks have returned to the ideas of Alan Boudreau [3–24]. For example, studies by Barkov and co-authors show a complex picture of variations in the composition of accessory apatite in different parts of the PGE-bearing Monchegorsk layered pluton. Accessory chlorapatite is developed in early ultramafic cumulates hosting the PGE reef, and fluorapatite crystallizes from the most fractionated portions of a melt in

 doi:10.20944/preprints202311.0074.v1



gabbroid rocks of the upper stratigraphic level of the pluton [3]. The F–Cl–OH diagram for the Monchegorsk apatite contains wide fields of solid solutions, represented by combinations of the components chlorapatite, hydroxylapatite and fluorapatite. Researchers of the Norilsk intrusions [18,21], studying wide variations of fluorine and chlorine in apatite of trap intrusions of the Siberian platform, suggest an important role of volatile components in melt differentiation and ore formation. In addition, the concentration of chlorine in apatite, as noted in studies [16,19], can be used as a discriminatory indicator for mafic-ultramafic rocks with copper-nickel mineralization.

Despite a whole series of mafic-ultramafic intrusions in which chlorapatite is present, PGE mineralization is not found in all of them [25]. In other cases, in the presence of significant ore concentrations of PGE, chlorapatite is not observed in rocks and ores [26,27]. Thus, a comparison of the currently available literature data suggests that the petrogenetic and prospecting value of apatite in connection with the distribution of PGE mineralization cannot be considered clear.

In this regard, an interesting question is about distribution and compositions of apatite in the Fedorova-Pana Layered Complex, the largest PGE ore object in the European part of the Arctic Zone of the Russian Federation, the host of four PGE deposits to date [27,28]. This article presents the results of studying apatite separated from a large-volume sample taken from anorthosites of the main ore body of the Kievey deposit in the West Pana intrusion and includes petrography of the mineralized anorthosite, EDS and LA-ICP-MS compositions and Raman spectroscopy of apatite.

## 2. Geological settings

Several dozen layered ultramafic-mafic intrusions of Paleoproterozoic age (2.50–2.45 Ga) are scattered across the territory of Fennoscandia [29]. Intrusions, occur generally in Archean rocks at borders with belts of Proterozoic supracrustal rocks. Taken in their entirety, these intrusions contain the full range of mineralization typical of layered intrusions, including chromite ores, sulfide cobalt-copper-nickel and PGE mineralization, and V-bearing titanomagnetite ores. Various types of PGE mineralization in these intrusions have attracted great interest in recent years. The main hosts of PGE mineralization are two Finnish, Penikat [30] and Portimo [31], and two Russian intrusions, Monchegorsk [32] and Fedorova-Pana [33]. The Portimo Igneous Complex and the Fedorova-Pana Layered Complex compete for the title of the largest PGE endowment in Europe [34,35]. From the point of view of studying the processes of PGE ore genesis the Fedorova-Pana Layered Complex is of undoubted interest regardless of the outcome of this competition. Petrologically, it is very important that Fedorova-Pana rocks retain a lot of traces of magmatic and post-magmatic processes due to less degree of metamorphic transformations limited mainly by the conditions of the greenschist facies along the contacts and tectonic faults. In addition, one can hardly fail to mention new minerals recently discovered in this complex: mitrofanovite $Pt_3Te_4$ named in honor of Academician F.P. Mitrofanov and [36] and panskiite $Pd_9Ag_2Pb_2S_4$ named after the Pana Tundra Ridge [37].

The Fedorova-Pana Complex consists of the Fedorova, Last'yavr, West Pana and East Pana intrusions (Figure 1). The main features of the geological structure and PGE mineralization of these intrusions are presented in the review [27]. All intrusions, except Last'yavr covered by swamps, contain PGE deposits, as well as several levels of poorly studied PGE mineralization. Recent studies show [38,39] that PGE mineralization is associated with four ore-magmatic systems (OMS), which are differently represented within the intrusions of the complex (Figure 1). The second OMS (Figure 1), considered as the main one, is represented in all intrusions in the form of PGE mineralization with an average Pd/Pt=4–6 and includes the Fedorova Tundra [27,40], North Kamennik [41] and Kievey deposits [42]. The East Chuarvy deposit located in the East Pana intrusion [43] belongs to the third OMS of higher platinum mineralization with Pd/Pt=2–3. The first and fourth OMS are relatively understudied and have Pd/Pt=8–12 and Pd/Pt<1 respectively. The former probably has the oldest U-Pb age of zircon in the Fedorova-Pana Complex, equal to 2509.4±6.2 Ma [44].

Preprints (www.preprints.org) | NOT PEER-REVIEWED | Posted: 2 November 2023 doi:10.20944/preprints202311.0074.v1



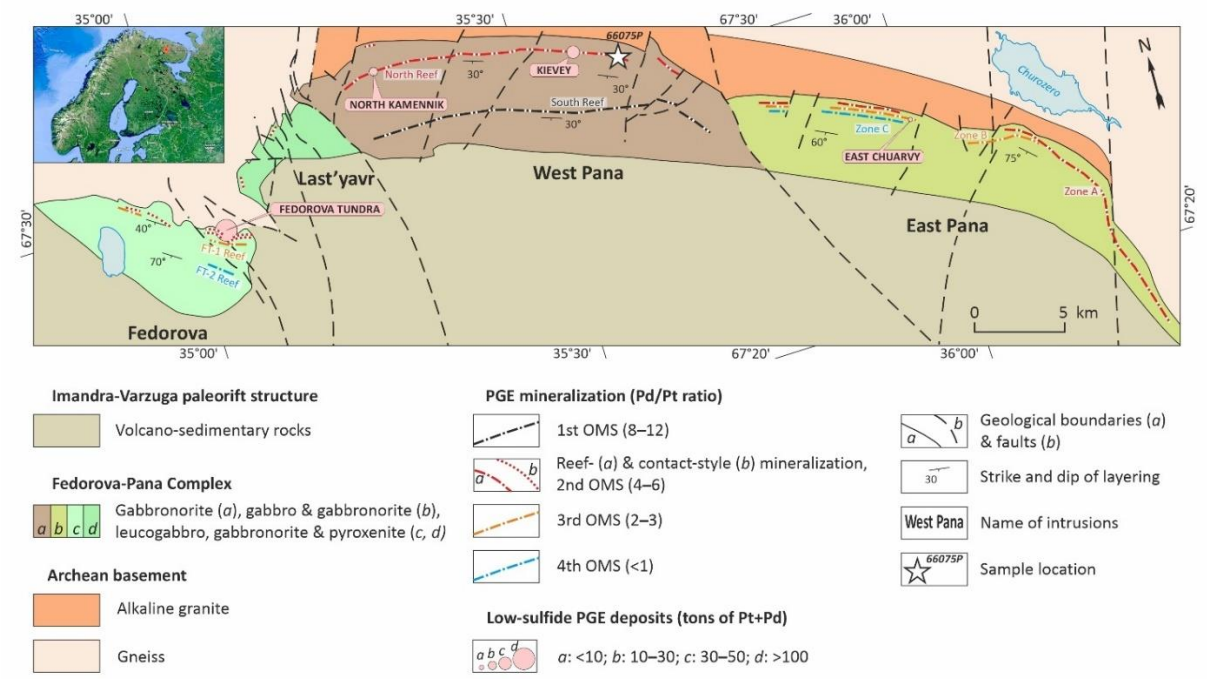


**Figure 1.** Schematic geologic map of the Fedorova-Pana Layered Complex. Modified after [27]. The inset shows Fennoscandia and the position of the complex on a google map. Abbreviation: OMS, ore-magmatic system; see text for explanation.

The Kievey deposit is a part of the North PGE Reef (Figure 1), localized in the Lower Layered Horizon of the West Pana intrusion. The Lower Layered Horizon overlies relatively homogeneous rocks of the Gabbronorite Zone 1 and overlain by equally homogeneous rocks of Gabbronorite Zone 2 (Figure 2). The horizon's structure is a cyclic alternation of orthopyroxenite-norite-gabbronorite-leucogabbro-anorthosite rock series with an averaged thickness of about 40 m. From two to five cycles can appear in different sections of the Lower Layered Horizon [42]. Each cycle can contain both a complete set of the rock series, as well as a reduced one, represented by gabbronorite-leucogabbro or gabbronorite with thin and rare layers of leucocratic composition. The formation of this magmatic sequence is associated with the replenishment of the magma chamber with a new portion of magma and the emergence of a hybrid melt, in which areas of continuous and discontinuous crystallization appear alternating along the strike of the temporary bottom of the chamber [45]. A reduced series of rocks forms in the case of continuous crystallization of plagioclase and pyroxenes. Discontinuous crystallization in the crystal-undersaturated interval between the crystallization zone and the temporary bottom of the chamber gives way to complete separation of plagioclase from orthopyroxene and formation of orthopyroxenite-anorthosite layering [46].

Preprints (www.preprints.org) | NOT PEER-REVIEWED | Posted: 2 November 2023 doi:10.20944/preprints202311.0074.v1



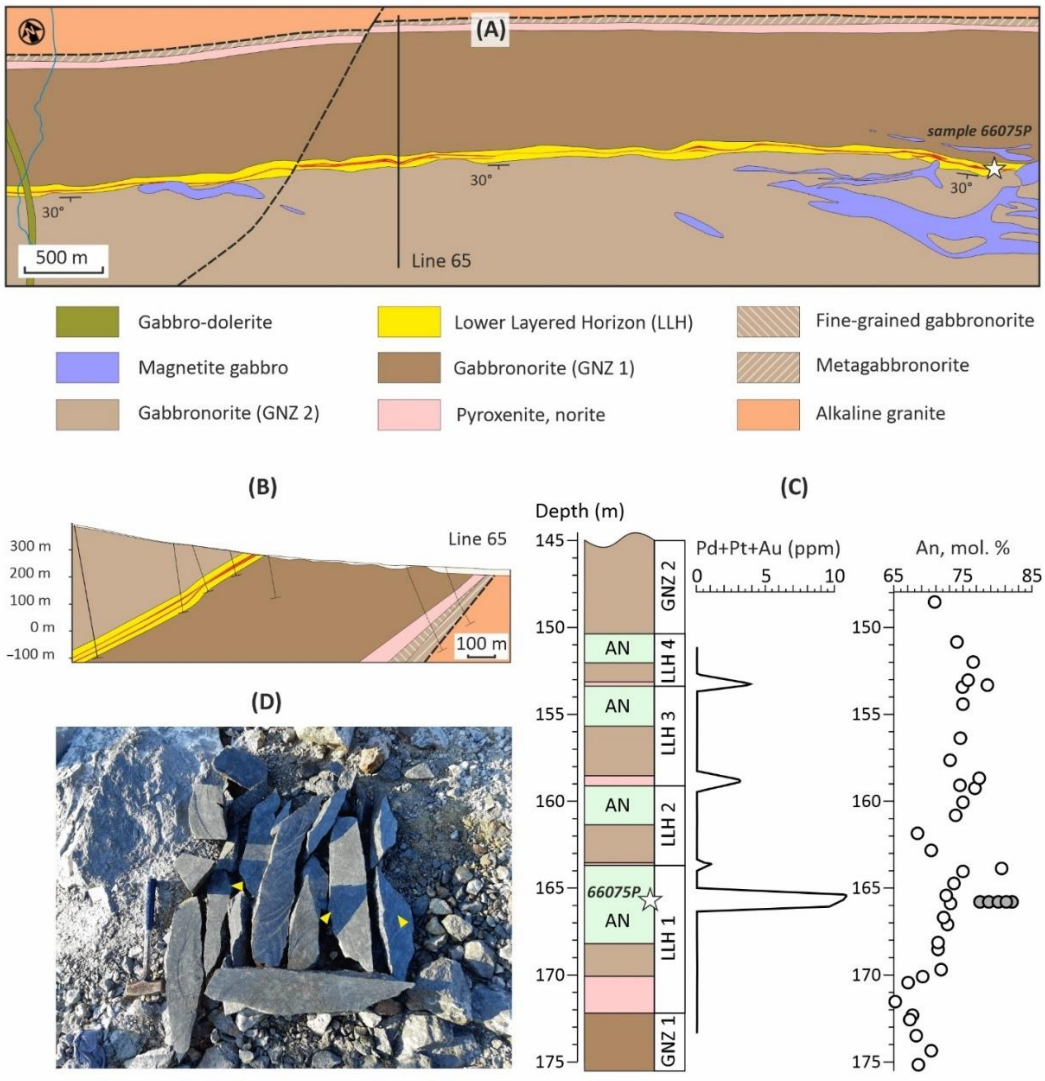


**Figure 2.** (A) Simplified geological map of the Kievey PGE deposit in the North Reef of the West Pana intrusion. Solid red lines show ore bodies. Modified from [42]. (B) Geological cross-section of the Kievey deposit along line 65. (C) Idealized and generalized section of the Kievey deposit. Based on data from drill hole 23 from [48] and added by data on the mineralized anorthosites from this study. White circles show An(norm.) content in plagioclase, calculated from whole-rock data [47], while gray circles correspond to compositions of plagioclase cores in the mineralized anorthosite. (D) Photo of the large-volume sample 66075P, which gave the accessory apatite concentrate. Yellow triangles indicate sulfide dissemination. Hammer length is 40 cm. Abbreviations: AN, leucogabbro and anorthosites; GNZ 1, Gabbronorite Zone 1; GNZ 2, Gabbronorite Zone 2; LLH, LLH 1, etc., Lower Layered Horizon and its cycles.

The North PGE Reef is a series of thin lens-shaped bodies of various rocks of the Lower Layered Horizon ("reef package") containing typically 2–5 vol. % of disseminated sulfides and PGE up to first tens of ppm (Figure 2). In many of its characteristics, primarily thickness, extent and PGE content, the North Reef is close to the well-known Merensky Reef in South Africa, as well as the JM Reef in the USA [42]. The North Reef is divided along its strike into several portions named after the neighboring mountain uplands of the Pana Tundra Ridge: 1) Kamennik, 2) Suleipakhk, 3) Kievey and 4) Peshempakhk. The reserves of base and precious metals at the Kievey site, as well as at the Kamennik site, are on the state balance sheet thanks to the joint efforts of academic organizations and companies [41,42]. PGE- and Au-enriched sulfide mineralization at the Kievey deposit is associated primarily with the second cycle of the Lower Layered Horizon, but in subsequent cycles PGE mineralization does not disappear and occurs in the form of more discontinuous lenses. Sulfides are

 doi:10.20944/preprints202311.0074.v1



mainly represented by pyrrhotite, chalcopyrite and pentlandite. The main PGE minerals are kotulskite, vysotskite, merenskyite, braggite, moncheite. In addition, mineralized rocks contain gold and Pd-pentlandite [42]. The main type of mineralized rocks is leucogabbro and anorthosites. According to ordinary sampling data these rocks make up 42% of the main ore body of the Kievey deposit [42]. As an interesting property of the North Reef it should be noted (Figure 2C) that each occurrence of mineralized rocks in the Lower Layered Horizon is accompanied by a maximum content of anorthite in plagioclase in contrast to the adjacent barren rocks [47].

## 3. Materials and methods

An apatite concentrate was separated from a large-volume sample 66075P (N 67.5067789994°; E 35.6361780044°; WGS 84) weighing 30 kg using technique described in [49]. The sample was taken from clearing in a small open pit from a layer of anorthosites and leucogabbro about 10 m thick. The southwestern dip of the layer at an angle of 30° is recorded in the outcrop by a trachyte-like structure, caused by the plane-parallel orientation of coarse plagioclase laths. Sulfide dissemination 3–7 vol. %, developed in the middle part of the layer and containing up to 25 ppm Pt+Pd+Au, was previously sampled using the diamond sawing during exploration of the deposit [50]. To collect the 66075P sample, the rock was resawed (Figure 2D). In addition, a 10x15x20 cm anorthosite ore block located nearby in the clearing was cut into five pieces to produce a 30x45x150 mm Ki-19-3ch-III sample, in which plane-parallel plagioclase laths are oriented almost orthogonally to the elongation of the sample (Figure S1). For an extended petrographic characterization, this sample was studied by X-ray computed tomography using a General Electric V|tome|X S 240 system (Germany) installed at the Kazan Federal University. Features of the tomography technique are given in [51].

An epoxy inch-sized polished section 66075P-1 was prepared from the apatite concentrate. Apatite grains from polished section 66075P-1 and from regular polished sections 66075, 66075-2 and 66075-3 were studied in detail using a Leo-1450 scanning electron microscope (Carl Zeiss) equipped with an Aztec UltimMax-100 energy-dispersive X-ray spectrometer (Oxford Instruments). Backscatter electron (BSE) images captured and all inclusions in apatite identified. The apatite grains were analyzed by X-ray electron probe energy dispersive (EDS) spectroscopy. Device operating parameters: accelerating voltage 20 kV, electronic probe current 300-500 nA in BSE mode and 2000 nA in EDS analysis mode. The following analytical lines (and reference substances) were used in the analysis: PK$\alpha$, CaK$\alpha$ and FK$\alpha$ (fluorapatite), SiK$\alpha$ (wollastonite), ClK$\alpha$ (atacamite), FeK$\alpha$ (hematite), SrL$\alpha$ (strontianite), MnK$\alpha$ ($MnCO_3$), LaL$\alpha$ (LaSe), CeL$\alpha$ (CeS), NdL$\alpha$ ($LiNd(MoO_4)_2$). The spectra accumulation time was 100 seconds. The results of apatite analysis are shown in Table S1.

The concentrations of trace elements in apatite were determined using laser ablation inductively coupled plasma mass spectrometry (LA-ICP-MS) on a Perkin Elmer NexION 300S spectrometer with an ESI NWR213 laser ablation attachment at the «Geoanalitik» Center for Collective Use of the IGG UB RAS (analyst V.S. Chervyakovsky). The measurements were carried out according to the method described in [52]. The results were processed in the GLITTER V4.4 program using the internal standard CaO. Glasses NIST SRM 610 and NIST SRM 612 were used as external standards. Trace element concentrations along with measurement uncertainty are given in Table S2.

Raman spectra for ten apatite grains from the sample 66075P-1 were obtained on an EnSpectr R532 spectrometer (Spektr-M, ISSP RAS, Chernogolovka, Russia) with an Olympus BX-43 microscope at the Mining Institute of the KSC RAS. Raman spectra were excited by a solid-state laser (532 nm) with an actual power of 18 mW under a 20× objective (NA 0.75). The spectra were obtained in the range of 170–4000 $cm^{-1}$ with a resolution of 5–8 $cm^{-1}$ at room temperature. To improve the signal-to-noise ratio, the number of acquisitions was set to 20. All spectra were processed using algorithms implemented in the OriginPro 8.1 software package (Originlab Corporation, Northampton, MA, USA).

Preprints (www.preprints.org) | NOT PEER-REVIEWED | Posted: 2 November 2023 doi:10.20944/preprints202311.0074.v1



## 4. Results

### *4.1. Petrography*

The mineralized anorthosite (Figure 3) is a coarse-grained cumulate containing 75–85 vol. % plagioclase with plane-parallel orientation or trachyte-like structure. Plagioclase mainly forms irregularly colored brownish grains of bytownite $An_{78–82}$ (Figure 2C) up to 6 mm in size with marginal parts of uncolored labradorite $An_{61–65}$. The coloration is apparently due to mechanical submicron inclusions of iron oxides, as in other rocks of the Fedorova-Pana Complex [53]. In the underlying barren anorthosite uncolored marginal areas of plagioclase are narrower and contain less anorthite component $An_{56–63}$, while in the mineralized anorthosite these plagioclase portions have considerable width, comprising up to one third of the whole grain.

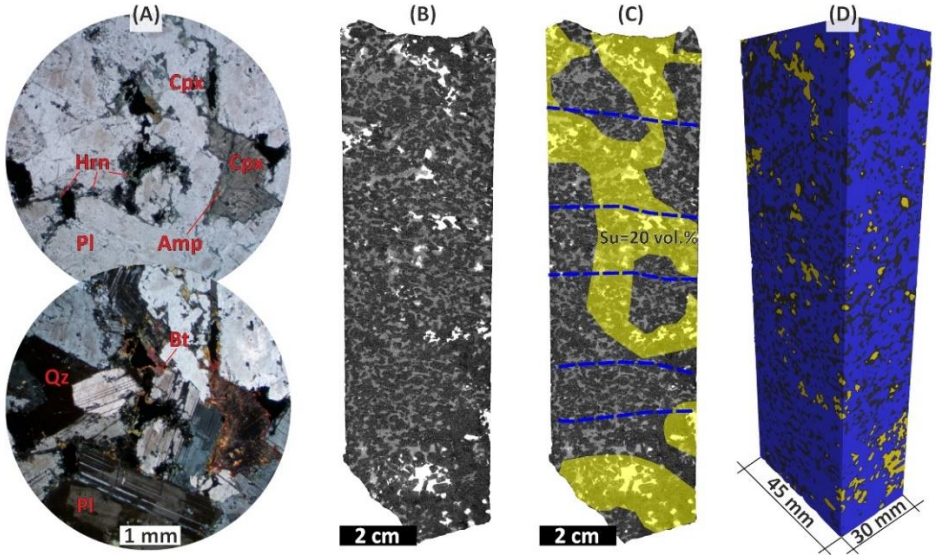


**Figure 3.** (A) Micro-photo for thin section 66075. (B, C) X-ray density section for sample Ki-19-3ch-III elongated across plane parallel orientation of plagioclase (dark); dashed blue lines in (C) indicate this plagioclase plane parallel orientation. (D) 3D visualization of main mineral phases in sample Ki-19-3ch-III: blue, plagioclase; grey, pyroxenes and amphibole; yellow, sulfides. Note that sulfides in the Ki-19-3ch-III sample have a regular distribution in the form of jets connected into one system; this can be seen from the relationship of the latter with the orientation of plagioclase.

The interstitial space is composed predominantly by amphibolized ortho- and clinopyroxene, as well as quartz, biotite, hornblende, sulfides, and magnetite (Figure 3).

The mineralized anorthosite contains 5–7 vol. % of disseminated sulfides having irregular distribution at first glance. The sulfides are pyrrhotite, pentlandite and chalcopyrite, often in association with magnetite. Sphalerite is extremely rare. In large samples of the rock (Figure S1), sulfide dissemination form interstitial "jets" in many places. These “jets” come across the trachyte-like structure, i.e., across the plane-parallel oriented plagioclase laths. An example of such "jets" is a sulfide percolation structure resembling the number eight (Figure 3B-D) as one can see on a 3D visualization of mineral phases on the results of X-ray computed tomography of the mineralized anorthosite sample.

Accessory minerals include apatite, baddeleyite, barite, ilmenite, clausthalite, titanite and zircon. Precious metal minerals occur as small micron-sized inclusions, mainly in silicates surrounding intergrowths of sulfide minerals. These include arsenopalladinite $Pd_8(As,Sb)_3$, vysotskite (Pd,Ni)S, vincentite $Pd_3As$, merenskyite $(Pd,Pt)(Te,Bi)_2$, moncheite $(Pt,Pd)(Te,Bi)_2$, kotulskite $Pd(Te,Bi)_{2-x}$, rusteburgite $(Pt,Pd)_3Sn$, telargpalite $(Pd,Ag)_3Te$, törnroosite $Pd_{11}As_2Te_2$ and others.

Preprints (www.preprints.org) | NOT PEER-REVIEWED | Posted: 2 November 2023 doi:10.20944/preprints202311.0074.v1



*4.2. Mineral assemblages, morphology, and internal structure of apatite*

Apatite in the mineralized anorthosite occurs in two assemblages: 1) together with plagioclase as small inclusions in the marginal parts of laths (Figure 4A) and 2) in association with interstitial minerals (Figure 4B). Apatite grains of the first association have sizes from 40 to 100 μm and are characterized by a short-prismatic euhedral habitus. Interstitial apatite has morphologically different, predominantly isometric grains ranging in size from 300 to 600 μm, in some cases up to 2.5 mm, when it can compose a whole interstitium between plagioclase laths (Figure 4B). Apatite grains are mostly homogeneous (Figure 4C), although in some of them at high contrast of BSE-images a weak zoning is noted (Figure 4D), apparently related to different REE concentrations.

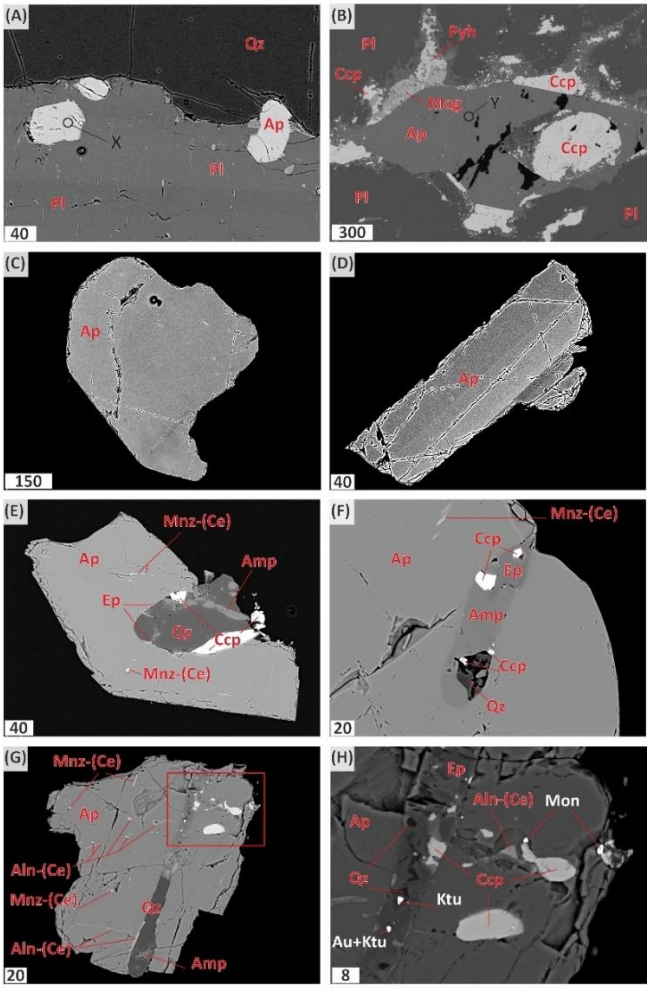


**Figure 4.** BSE images of apatite from the mineralized anorthosite of the Kievey PGE deposit. (A) Thick section 66075-2. X spot shows the most fluorine composition of apatite among the studied grains. (B) Thick section 66075. Y spot corresponds the least fluorine apatite in the mineralized anorthosite. (C–H) Polished epoxy mount with the apatite concentrate. Note that one can see grains of noble metal minerals in image (H): moncheite (Pt,Pd)(Te,Bi)$_2$, kotulskite Pd(Te,Bi)$_{2-x}$ and gold. Mineral abbreviations after [54]. Scale bar is in μm.

Apatite grains often contain tiny 1–2 μm inclusions of allanite-(Ce) and monazite-(Ce) (Figure 4E-G). In addition to these minerals, silicate, and chalcopyrite-silicate inclusions 10–30 μm in size, as well as thin chalcopyrite veinlets are noted in several apatite grains. One grain containing such inclusions has tiny phases of noble metal minerals, namely kotulskite, moncheite and gold (Figure 4H).

 doi:10.20944/preprints202311.0074.v1



*4.3. Apatite composition*

Representative EDS analyses of accessory apatite from polished section 66075P-1 are summarized in Table 1. The full data set of major elements in apatite from the studied polished sections (Table S1) shows that CaO content generally ranges from 54.3 to 55.9 wt. %, decreasing to 51.0 wt. % in rare zones of secondary alteration. The $P_2O_5$ content ranges from 40.3 to 42.6 wt. %. Systematic admixtures of $SiO_2$ (0.1–0.7 wt. %) and FeO (up to 0.4 wt. %) are observed in apatite. Most apatite grains contain $Ce_2O_3$ (up to 0.5 wt. %); some grains include $La_2O_3$ (up to 0.2 wt. %) as well as $Nd_2O_3$ (up to 0.4 wt. %). Strontium, whose concentration in apatite is below the detection limit of the EDS analyzer (Table S2), is not detected by regular analysis, reflecting severe depletion of residual liquid due to mass incorporation of strontium into plagioclase. In contrast to apatite from the mineralized anorthosite, apatite from the overlying rocks of the Lower Layered Horizon may contain up to 0.15 wt. % SrO [62]. Measured volatile components in apatite are F and Cl. Their concentrations reach 2.21 and 0.46 wt. %, respectively (Table S1). The most fluorine apatite belongs to the first assemblage.

**Table 1.** Representative analyzes of apatite from the ore-bearing anorthosite of the Lower Layered Horizon in the West Pana intrusion (sample 66075P-1).

| Spots | 1b1 | 1c-2-3 | 3b | 3d | 4a2 | 4d1 | 4d2 | 5a1 | 5c2 | 6a1 |
|---|---|---|---|---|---|---|---|---|---|---|
| CaO | 54.35 | 54.49 | 55.09 | 55.06 | 55.00 | 54.83 | 55.23 | 54.62 | 55.26 | 54.54 |
| FeO | 0.06 | 0.06 | 0.07 | 0.13 | 0.05 | 0.10 | 0.07 | 0.10 | 0.08 | 0.07 |
| $La_2O_3$ | 0.12 | bdl | bdl | 0.12 | bdl | bdl | bdl | bdl | bdl | 0.08 |
| $Ce_2O_3$ | 0.39 | 0.14 | 0.16 | 0.25 | 0.20 | 0.23 | 0.18 | 0.36 | 0.22 | 0.30 |
| $Nd_2O_3$ | bdl | bdl | bdl | bdl | bdl | bdl | bdl | bdl | bdl | 0.13 |
| $P_2O_5$ | 41.26 | 41.33 | 41.88 | 42.09 | 41.80 | 41.74 | 42.04 | 41.58 | 42.16 | 41.64 |
| $SiO_2$ | 0.38 | 0.21 | 0.21 | 0.25 | 0.26 | 0.26 | 0.22 | 0.39 | 0.25 | 0.29 |
| F | 1.53 | 1.17 | 1.44 | 1.41 | 1.51 | 1.09 | 1.38 | 1.53 | 1.45 | 1.42 |
| Cl | 0.03 | 0.14 | 0.11 | 0.17 | 0.10 | 0.46 | 0.34 | 0.29 | 0.25 | 0.15 |
| O=F,Cl | 0.65 | 0.52 | 0.63 | 0.63 | 0.66 | 0.56 | 0.66 | 0.71 | 0.67 | 0.63 |
| Сумма | 97.47 | 97.02 | 98.33 | 98.85 | 98.26 | 98.15 | 98.80 | 98.16 | 99.00 | 97.99 |
| Formula coefficients | | | | | | | | | | |
| Ca | 4,88 | 4.92 | 4.90 | 4.87 | 4.89 | 4.90 | 4.89 | 4.87 | 4.88 | 4.87 |
| Fe | 0.00 | 0.00 | 0.00 | 0.01 | 0.00 | 0.01 | 0.00 | 0.01 | 0.01 | 0.00 |
| La | 0.00 | 0.00 | 0.00 | 0.00 | 0.00 | 0.00 | 0.00 | 0.00 | 0.00 | 0.00 |
| Ce | 0.01 | 0.00 | 0.00 | 0.01 | 0.01 | 0.01 | 0.01 | 0.01 | 0.01 | 0.01 |
| Nd | 0.00 | 0.00 | 0.00 | 0.00 | 0.00 | 0.00 | 0.00 | 0.00 | 0.00 | 0.00 |
| P | 2.93 | 2.95 | 2.94 | 2.94 | 2.94 | 2.95 | 2.94 | 2.93 | 2.94 | 2.94 |
| Si | 0.03 | 0.02 | 0.02 | 0.02 | 0.02 | 0.02 | 0.02 | 0.03 | 0.02 | 0.02 |
| F | 0.41 | 0.31 | 0.38 | 0.37 | 0.40 | 0.29 | 0.36 | 0.40 | 0.38 | 0.37 |
| Cl | 0.00 | 0.02 | 0.02 | 0.02 | 0.01 | 0.07 | 0.05 | 0.04 | 0.03 | 0.02 |
| OH | 0.59 | 0.67 | 0.61 | 0.61 | 0.59 | 0.65 | 0.59 | 0.56 | 0.59 | 0.60 |

Note. SrO and MnO are below detection limit (bdl), not shown in the table. The formulas were calculated based on 25 negative charges.

A typical Raman spectrum of apatite from this study is shown in Figure 5, while its interpretation based on numerous literature data [55–60] is shown in Table 2. Most of the bands that appear on the spectrum correspond to various types of $PO_4$ vibrations. The band at 1079 $cm^{-1}$ can correspond to both $PO_4$ vibrations (ν3 asymmetric stretching) and $CO_3$ vibrations (ν1 plane stretching) with isomorphic B-type substitutions ($PO_4 \rightarrow CO_3$). The broad band at ≈ 3565 $cm^{-1}$ corresponds to the vibrations of the OH-group, which allows us to calculate an apatite formula according to the scheme given in Table 1.

Preprints (www.preprints.org) | NOT PEER-REVIEWED | Posted: 2 November 2023 doi:10.20944/preprints202311.0074.v1



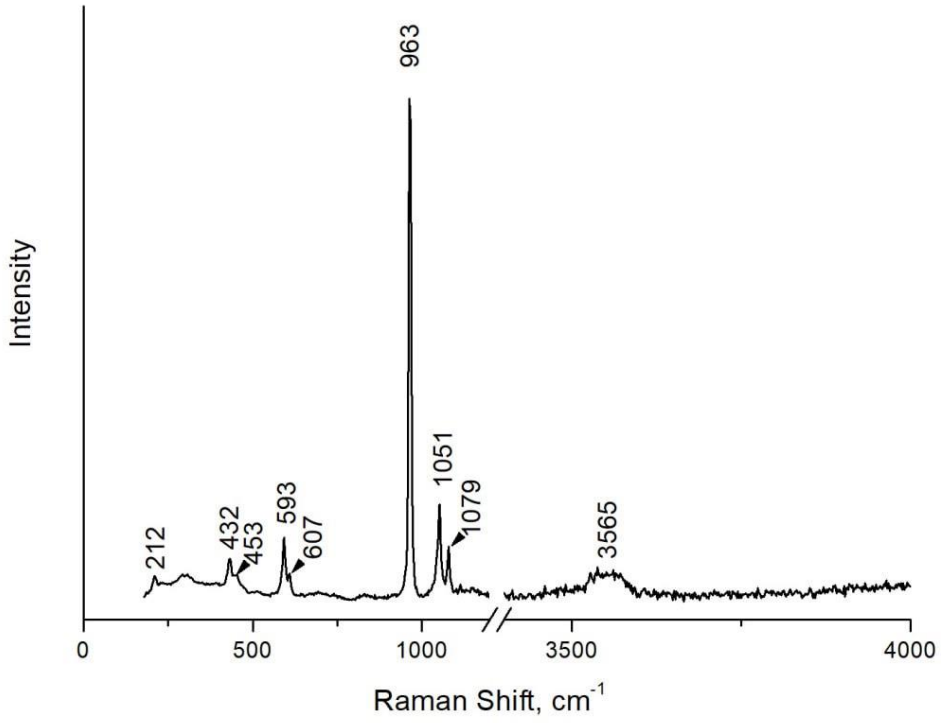


**Figure 5.** Typical Raman spectrum of apatite from the mineralized anorthosite of the Kievey deposit.

**Table 2.** Raman bands in apatite from the mineralized anorthosite of the Kievey deposit.

| Raman Shift, $cm^{-1}$ | Band assignments |
|---|---|
| 212 | Lattice mode |
| 432 | ν2 bending mode |
| 453 | |
| 593 | ν4 $PO_4$ triply degenerate bending mode |
| 607 | |
| 963 | ν1 $PO_4$ symmetric stretching mode |
| 1051 | ν3 $PO_4$ triply degenerate asymmetric stretching mode |
| 1079 | ν1 $CO_3$ (C-O in plane stretch) / ν3 $PO_4$ asymmetric stretching |
| 3565 | OH vibration band |

In the Cl-F-OH diagram (Figure 6), apatite compositions from the mineralized anorthosite form a compact field elongated along the F-OH side. The relatively more euhedral and high-F apatite included in the plagioclase obviously formed before the interstitial one (compare compositions X and Y in Figure 6A). Consequently, apatite in the studied rock evolves according to the fluorapatite-hydroxylapatite trend shown in Figure 6A by the pink dashed line. These results give strong evidence that the mineralized anorthosites from the main ore body of the Kievey PGE deposit does contain apatite with extremely low chlorine contents. However, it should be noted that fluorapatite and hydroxylapatite from the upper cycles of the Lower Layered Horizon contains an increased amount of chlorine with the maximum concentration in apatite from mesocratic and melanocratic rocks (Figure 6B).

Preprints (www.preprints.org) | NOT PEER-REVIEWED | Posted: 2 November 2023 doi:10.20944/preprints202311.0074.v1



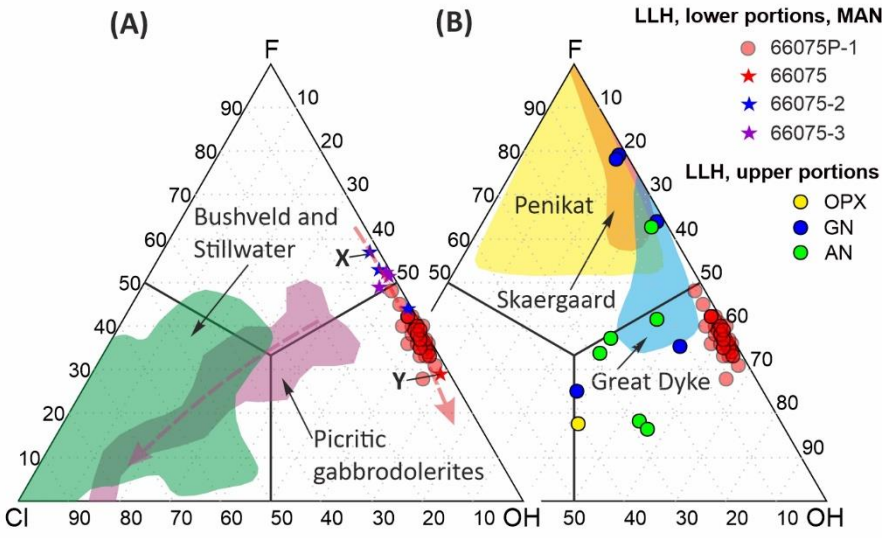


**Figure 6.** Triangular Cl-F-OH plot for apatite from various ultramafic-mafic intrusions in comparison with the mineralized anorthosites of the Kievey PGE deposit. (A) Bushveld and Stillwater complexes [1], as well as picritic gabbrodolerites of the Kharaelakh intrusion [61], the apatite compositions of which form the "platinum reactor" trend shown by the dashed purple line. The pink dashed line shows the trend of apatite compositions in mineralized anorthosites, starting with grain X and ending with grain Y in Figure 4. Note that composition Y is excluded from Table S1 due to low $P_2O_5$ content. (B) Penikat, Skergaard and Great Dyke intrusions [1] and the upper rhythms of the Lower Layered Horizon of the West Pana intrusion from the R.M. Latypov's thesis [62]. Abbreviations: AN, anorthosite; GN, gabbronorite; LLH, Lower Layered Horizon; MAN, mineralized anorthosite; OPX, orthopyroxenite.

As shown by the trace element data (Table S2), apatite from the mineralized anorthosite contains from 4059 to 5623 ppm total rare earth elements (REE); these variations determine the weak zoning in the grains that appears in high-contrast BSE images. The chondrite-normalized REE, Sr and Y patterns (Figure 7A) are characterized by a stable negative slope with an average $La/Yb_N$ ratio of 11.78, as well as negative Sr/Sr* and Eu/Eu* anomalies averaging 0.01 and 0.06, respectively. According to trace elements the apatite corresponds to intrusive mafic rocks (Figure 7B), although its compositions localized at the boundary with a field of rocks of high degrees of metamorphism. Compared to sulfide-bearing layered complexes, apatite from the mineralized anorthosite stands out from their composition fields, mainly due to low strontium concentrations (Figure 8).

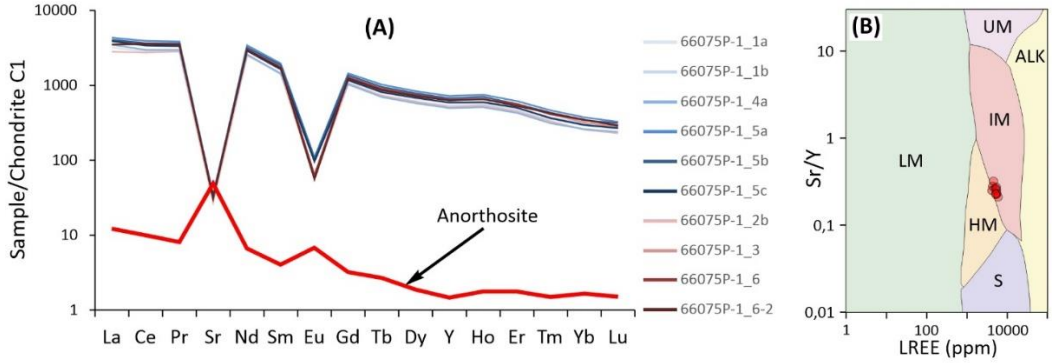


**Figure 7.** (A) Chondrite-normalized [63] variation diagrams for REE, Sr, and Y for apatite from the mineralized anorthosite of the Kievey PGE deposit. Whole-rock trace element contents are taken from [48]. (B) Binary diagram LREE vs. Sr/Y. Fields of composition from [8]. Abbreviations: ALK, alkali-rich igneous rocks; IM, mafic I-type granitoids and mafic igneous rocks; LM, low- and medium-grade metamorphic and metasomatic rocks; HM, partial-melts/leucosomes/high-grade

Preprints (www.preprints.org) | NOT PEER-REVIEWED | Posted: 2 November 2023 doi:10.20944/preprints202311.0074.v1



metamorphic rocks; S, S-type granitoids and high aluminum saturation index 'felsic' I-types rocks; UM, ultramafic rocks including carbonatites, lherzolites and pyroxenites.

Apatite grains containing sulfide and sulfide-silicate inclusions are depleted in chalcophile elements relative to grains without such inclusions, indicating the syngenetic formation of apatite and sulfides. For example, Ni content in the former varies from 0.46 to 1.63 ppm, while in grains without inclusions it reaches 81.55 ppm (Table S2).

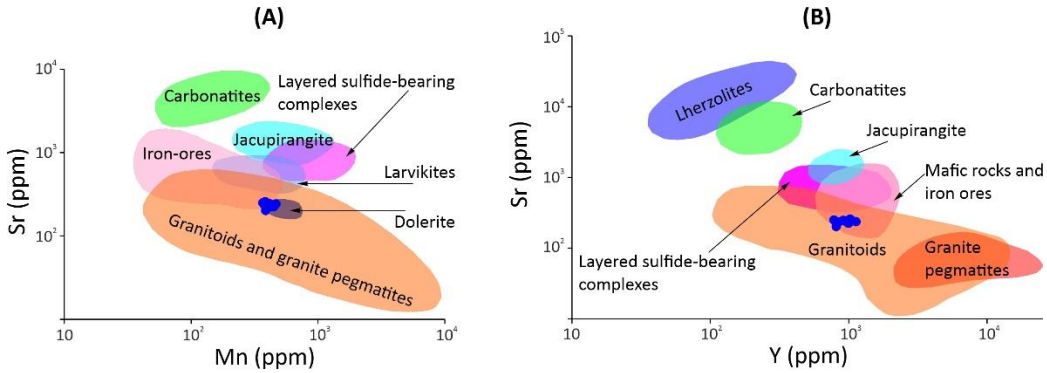


**Figure 8.** Binary discrimination diagrams Mn vs. Sr (A) and Y vs. Sr (B) for apatite from the mineralized anorthosite of the Kievey deposit (blue circles) in comparison with apatite from different geological settings. Composition fields are taken from [13,19,24,64].

## 5. Discussion

### *5.1. Nature of apatite in the mineralized anorthosite*

Apatite contents can vary by an order of magnitude in layered intrusions. In the most evolved rocks, such as those in the Bushveld [12], apatite is often a cumulus mineral in tens of percent abundance. On the other hand, in most layered intrusion rocks, late magmatic apatite occurs in fractions of a percent or as an accessory mineral in the form of small grains associated with quartz, biotite, feldspar, magnetite and sulfides in the interstices between plagioclase and pyroxene. In magmatic systems subjected to intense fluid reworking, for example in the Norilsk intrusions [21], post-magmatic generations of apatite are established by growth structures on late magmatic apatite.

The mineralized anorthosite contains 0.03 wt. % $P_2O_5$ [48] and the concentration of apatite in it corresponds to the accessory amount. The homogeneity of composition and low Sr content shows that apatite is represented by a single generation, crystallized from a melt that arose after mass crystallization of plagioclase. The key question is: is the apatite from the mineralized anorthosite a product of crystallization of the original trapped liquid of plagioclase cumulates or is it formed from sulfide-bearing interstitial melt migrating downward from the upper cycles of the Lower Layered Horizon? This question is not clearly answered at this stage of the study. The close association of apatite and ore material, including noble metal minerals, indicates the possibility of apatite infiltration together with sulfide liquid from the upper cycles. As possible additional evidence of the infiltration nature of apatite is some depletion of chalcophile elements in the apatite grains with sulfide inclusions (Table S2).

### *5.2. What conclusions about the indicator role of apatite for the genesis of PGE mineralization can be drawn from the example of mineralized anorthosites of the Kievey deposit?*

In the context of comparison of PGE mineralization of Fennoscandian layered intrusions with their better known world analogues, which was repeatedly carried out at the stage of prospecting works [50], the fact of low-chlorine apatite dominance in the North Reef ore seems very interesting, since it contradicts one of the prospecting criteria developed on the examples of Bushveld and

 doi:10.20944/preprints202311.0074.v1



Stillwater. Unlike the Merensky Reef in the Bushveld, for example, there is high-grade PGE ore in the anorthosites of the Kievey deposit, but no chlorapatite at all. Why?

Trying to give an answer, one can draw an analogy with the taxitic gabbrodolerites of the Kharaelakh intrusion [61], containing up to 5 ppm PGE and apatite with a low chlorine content. At the same time, the disseminated sulfide mineralization in the picritic gabbrodolerites located higher in the section, containing up to 8 ppm PGE, and low-sulfide PGE mineralization in the amygdaloid rocks of the Kharaelakh intrusion with PGE concentrations up to 200 ppm [17], both contain chlorine-enriched apatite, including chlorapatite. As it seems to us, this effect can be explained by sulfide liquid percolation from the "platinum reactor" level [61], that is from the picritic gabbrodolerites through the taxitic gabbrodolerites towards the thick massive sulfide ore bodies [65]. A similar phenomenon, but on a different scale, we probably see in the mineralized anorthosites of the Kievey deposit.

Thus, it can be assumed that the mineralized anorthosites of the Kievey deposit provide another example of the infiltration sulfide mineralization containing sulfide liquid, the process of enrichment of which with noble metals did not occur *in situ*.

### *5.3. The role of post-magmatic processes for PGE mineralization in the Fedorova-Pana Complex*

The Fedorova-Pana Complex is generally poorly metamorphosed with post-magmatic mineral content not exceeding 10 vol. % in 70 % of its area. However, it was noticed that ore-bearing horizons are usually metamorphosed more strongly than the surrounding barren rocks where one can observe only green-shist metamorphic mineral assemblages. In this regard, the question of the role of post-magmatic processes in the formation of PGE mineralization arose [66–68]. Some contradiction has appeared in the ideas about the genesis of PGE mineralization. On the one hand, PGE mineralization in the West Pana and East Pana intrusions is clearly associated with extended layered bodies, that is, it belongs to the reef type and is of magmatic origin. On the other hand, the mineralization is associated with zones of higher metamorphic alteration, but an influence of metamorphism on PGE mineralization formation is not clear except the fact of spatial connection.

To clarify this question, Voloshina and her colleagues conduct special studies [66–68]. These works have shown that metamorphic mineral assemblages of rocks in layered horizons and garnet-hornblende metasomatites surrounding some PGE mineralization correspond in P-T parameters to epidote-amphibolite and amphibolite facies [68]. These metamorphic assemblages are exclusively in spatial connection with layered ore-bearing horizons making researchers hypothesize regarding metamorphic genesis for Fedorova-Pana PGE mineralization [68]. This is partly confirmed by data on platinum group minerals (PGM) mineralogy [69], which show that the formation of the most late PGM is associated with the remobilization of PGE and the transformation of previously crystallized PGM under the influence of fluid. Besides, ore-bearing rocks have higher concentrations of almost all fluid components, especially $H_2S$, $SO_2$ and $CH_4$, although water is the main component (from 90 to 99 mol. %) of the fluid phase of the West Pana rocks [70]. Thus, thoughts about the metamorphic origin for PGE mineralization of the Fedorova-Pana Complex have been repeatedly discussed in the literature, despite the dominance of the magmatic model [28].

In the context of the large-scale infiltration of interstitial melt together with sulfide and PGE mineralization discussed here, we suggest that the presence of amphibolite facies mineral assemblages near the Lower Layered Horizon of the West Pana intrusion can be a result of the influence of the infiltrate passing through the rocks.

### *5.4. Model of the formation of PGE mineralization in anorthosites of the Kievey deposit*

The mechanism of formation of the Kievey PGE deposit cannot be considered separately from the processes of formation of various rocks of the Lower Layered Horizon, which hosts the North Reef. As noted above, the zone of discontinuous crystallization that occurs near the bottom of the crystallizing magma chamber above the cumulates may be responsible for the formation of the pyroxenite-gabbronorite-anorthosite layering, which appears and disappears along the strike of the horizon [45]. This zone is thought to occur in response to the influx of a new magma portion into the

 doi:10.20944/preprints202311.0074.v1



chamber, as has been suggested for the critical zones of many layered intrusions [71,72]. In the case of the Lower Layered Horizon, the composition of this new portion is close to the primary composition of the magma of the West Pana intrusion [46]. In addition, the cyclic structure of the horizon is assumed [42] to be the result of several such magmatic pulses. In contrast to the melanocratic cumulates of all overlying cycles, sulfide mineralization is never noted in the thickest one to two-meter orthopyroxenite layer at the base of the first cycle. Thus, the influx of a new portion of magma, which triggered the formation of layering, is split into a series of pulses, the first of which is barren, while all subsequent ones bring PGE-enriched sulfide liquid.

Taking this into account, the model for the formation of the Kievey deposit is presented schematically in the following form (Figure 9). To get an idea of the processes occurring in the magma chamber, let us imagine a magma with plagioclase and two pyroxenes crystallizing from bottom to top and forming a triple allotriomorphic-granular gabbronorite cumulate (stage I) which underlies the layered horizon now. The formation of the horizon starts because of the influx of slightly hotter magma of similar composition and the occurrence of areas with breaks in mineral crystallization, as well as areas where the crystallization zone is undersaturated with crystals, in which gravitational differentiation is stimulated and orthopyroxene, plagioclase-pyroxene, and plagioclase cumulate of the first cycle are formed (stage II). The continuation of this process resembles its beginning, with the difference that subsequent magmatic pulses contain sulfide liquid, probably partially enriched in PGE in an intermediate chamber [38]. The sulfide liquid, together with orthopyroxene crystals, settles inside the crystallization zone of these influxes and, possibly, its additional enrichment with PGE occurs in situ (stages III–IV). It should be noted that the rocks of the ore-bearing magmatic influxes contain apatite with elevated chlorine (Figure 6B). In this case, the sulfide and fluid-enriched intercumulus liquid percolates into the still hot plagioclase cumulates of the underlying cycle, leaving traces of this process in the interstices under the conditions of amphibolite facies and regular percolation textures in rocks. Thus, in the studied sample one can see discontinuous chains of sulfides, for example, folded into the elongated figure eight oriented across the plane-parallel laths of plagioclase (Figure 3). It is very characteristic that sulfide PGE mineralization of infiltration nature contains apatite depleted in chlorine, which indicates the possibility of considering the low chlorine content in apatite as a petrogenetic indicator of the infiltration process. Eventually, continuous crystallization of ternary cumulates resumes after the products of the last additional magmatic influx have solidified (stage V).

Preprints (www.preprints.org) | NOT PEER-REVIEWED | Posted: 2 November 2023 doi:10.20944/preprints202311.0074.v1



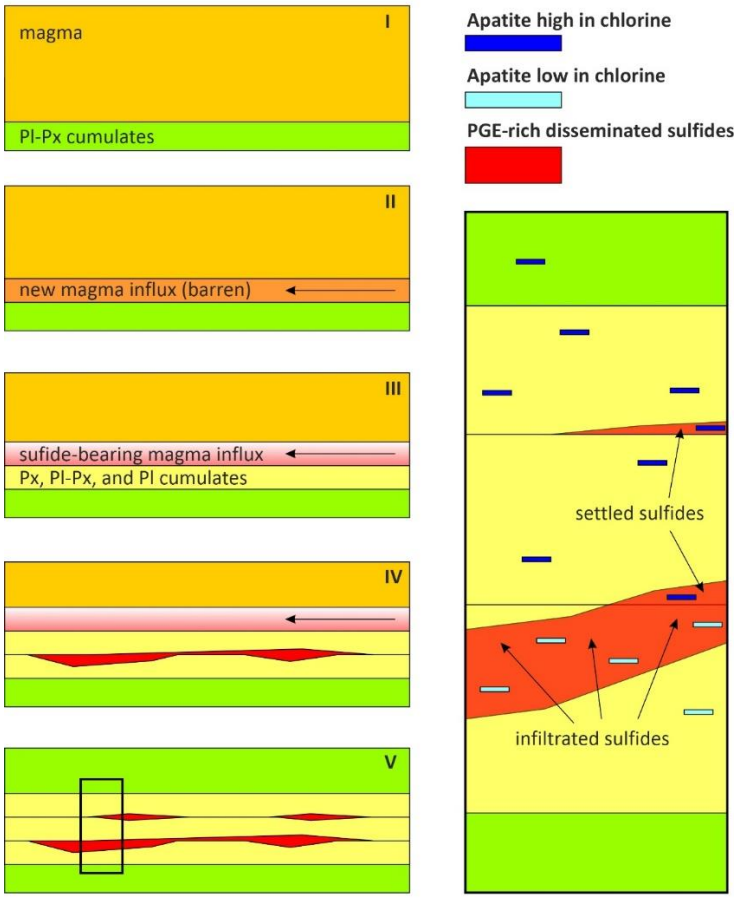


**Figure 9.** Simplified formation model for the Kievey PGE deposit. See text for further explanation of stages I–V.

*5.5. Critique of the sulfide percolation model*

The model of sulfide percolation in the mineralized anorthosite presented here is largely the result of the authors' close experience of the Kievey deposit studying, starting from the prospecting stage of its study, and ending with the preparation of the geological part of the report with calculating reserves. A weakness of this model is the following point. For a reasonable statement of the percolation of sulfide or sulfide-silicate substance through the pore space of cumulates, it is necessary, first, to characterize the composition of this substance, which requires a more detailed petrographic study of both the possible source and the rocks into which the ore substance percolated, including the rocks not affected by this process. Special attention, in our opinion, is required to plagioclase and composition of its rims. While a detailed petrographic study remains a matter of the future, another counterargument for the model is the spatial coincidence of the position of the mineralized anorthosite in the section and the maximum of the anorthite component in plagioclase (Figure 2C), which indicates the connection of mineralization and some early magmatic process. In addition, this study has chances to obtain more strong evidence by comparing the petrographic features of different facies of the reef represented not on the generalized section (Figure 2C), but on several real sections where the inferred infiltration process is represented in different degrees. It should be noted that presumably seep-associated disseminated sulfides within the North Reef are known in another of its deposits to the west (North Kamennik, Figure 1). These sulfides may form ore bodies located approximately ten meters below the footwall of the Lower Layered Horizon [73].

The theoretical possibility of sulfide melts migration is also one of the most difficult and controversial issues of petrology, concerning not only PGE-Cu-Ni sulfides formation, but also the processes of mantle-core separation [74]. For instance, Barnes and colleagues concluded [74] that the ability of sulfide liquids to migrate through the pore space of olivine cumulates is limited. However,

 doi:10.20944/preprints202311.0074.v1



we do not take this issue off the table for the mineralized anorthosites, because the problem this time is migration through the pore space of coarse-grained plagioclase cumulates, and migration of a sulfide-silicate mixture rather than so much sulfide liquid.

## 6. Conclusions

To summarize the attempt made to present the Kievey PGE deposit to a global petrologic audience, it is necessary to reiterate several points. The Kievey deposit is a part of the North PGE Reef of the West Pana intrusion. The reef is located within the Lower Layered Horizon consisting of several cycles of the orthopyroxenite-norite-gabbronorite-anorthosite series and is associated with the cyclic units following the first one. In the studied area, PGE-enriched sulfide mineralization representing the main ore body of the deposit occurs in anorthosites of the lower cyclic unit and is characterized by a series of features indicating its infiltration origin. The most striking of them are 1) location of mineralization in the middle part of the anorthosite layer in proximity (about 5 m) to melanocratic rocks of the overlying cycle, also containing PGE mineralization, which can be considered as a source, and 2) intersecting position of sulfide or sulfide-silicate "jets" in relation to the plane-parallel texture of plagioclase cumulate. At the same time, the location of sulfide mineralization in areas with maximum anorthite content in plagioclase of the Lower Layered Horizon indicates that the ore formation is related to an early magmatic process. Additional petrographic studies, especially in comparison between several detailed sections of the reef, may help to develop a more consistent scenario for the formation of mineralization.

The apatite group minerals in the ore-bearing anorthosite are represented by late magmatic interstitial low-chlorine apatite, containing only 0.46 wt. % Cl and closely associated with both platinum minerals and sulfides. Our detailed studies allow to establish the trend in the direction from fluorapatite to hydroxylapatite despite of studying of a single rock type only. Apatite has low REE and Sr contents reaching up to 5623 ppm and 257 ppm respectively. The chondrite-normalized patterns show a moderate enrichment in LREE with $La/Yb_N$=11.78, as well as pronounced negative anomalies Sr/Sr*=0.01 and Eu/Eu*=0.06. The obtained data on the concentration of trace elements in apatite expand the known fields of apatite compositions from ore-bearing layered intrusions at the expense of the anorthosite, which is apparently studied for the first time by laser ablation.

In the context of discussing the indicator role of chlorapatite in the formation of PGE mineralization, it should be noted that a presence of low-chlorine apatite in mineralized rocks can be considered as an indication that enrichment of sulfide liquid in PGE occurred at another level of the ore-magmatic system, i.e., not in situ. In the case of the main ore body of the Kievey deposit, this process could occur during crystallization of the overlying cycles of the Lower Layered Horizon or in an intermediate chamber at depth.

**Supplementary Materials:** The following supporting information can be downloaded at: www.mdpi.com/xxx/s1, Figure S1: Photographs of a mineralized anorthosite ore block from the Kievey deposit; Table S1: Composition of apatite from rocks of the Kievey PGE deposit (EDS); Table S2: Trace element concentrations in apatite from the mineralized anorthosite of the Kievey PGE deposit (LA-ICP-MS); Table S3: Minimum detection limits (ppm, 99% confidence) for LA-ICP-MS spots.

**Author Contributions:** Conceptualization, A.S. and N.G.; methodology, N.G.; software, A.S.; validation, A.S., N.G. and T.R.; formal analysis, T.R.; investigation, A.S. and Ye.S.; resources, N.G.; data curation, A.K. and Ye.S.; writing—original draft preparation, A.S. and T.R.; writing—review and editing, A.S. and N.G.; visualization, A.S. and N.G.; supervision, N.G.; project administration, N.G.; funding acquisition, A.S. and N.G. All authors have read and agreed to the published version of the manuscript.

**Funding:** The work was carried out with the financial support of the Russian Science Foundation Project No. 22-27-20106, https://rscf.ru/project/22-27-20106/.

**Data Availability Statement:** The data presented in this study are available in Supplementary.

**Acknowledgments:** The authors are grateful to R.I. Kadyrov (KFU, Kazan) for computed tomography of the mineralized anorthosite and V.S. Chervyakovsky (IGG UB RAS, Yekaterinburg) for LA-ICP-MS results for apatite.

**Conflicts of Interest:** The authors declare no conflict of interest. The funders had no role in the design of the study; in the collection, analyses, or interpretation of data; in the writing of the manuscript; or in the decision to publish the results.

## References

1. Boudreau, A.E.; Mathez, E.A.; McCallum, I.S. Halogen Geochemistry of the Stillwater and Bushveld Complexes: Evidence for Transport of the Platinum-Group Elements by Cl-Rich Fluids. *J. Petrol.* **1986**, *27*, 967–986.
2. Boudreau, A.E. Chlorine as an Exploration Guide for the Platinum-Group Elements in Layered Intrusions. *J. Geochemical Explor.* **1993**, *48*, 21–37, doi:https://doi.org/10.1016/0375-6742(93)90080-6.
3. Barkov, A.Y.; Sharkov, E. V; Nikiforov, A.A.; Korolyuk, V.N.; Sil'yanov, S.A.; Lobastov, B.M. Compositional Variations of Apatite and REE-Bearing Minerals in Relation to Crystallization Trends in the Monchepluton Layered Complex (Kola Peninsula). *Russ. Geol. Geophys.* **2021**, *62*, 427–444.
4. Barkov, A.Y.; Nikiforov, A.A. Compositional Variations of Apatite, Fractionation Trends, and a Pge-Bearing Zone in the Kivakka Layered Intrusion, Northern Karelia, Russia. *Can. Mineral.* **2016**, *54*, 475–490, doi:10.3749/canmin.1500035.
5. Sadove, G.; Konecke, B.A.; Fiege, A.; Simon, A.C. Structurally Bound S2-, S1-, S4+, S6+ in Terrestrial Apatite: The Redox Evolution of Hydrothermal Fluids at the Phillips Mine, New York, USA. *Ore Geol. Rev.* **2019**, *107*, 1084–1096.
6. Raič, S.; Mogessie, A.; Krenn, K.; Hauzenberger, C.A.; Tropper, P. Deciphering Magmatic and Metasomatic Processes Recorded by Fluid Inclusions and Apatite within the Cu--Ni$\pm$PGE-Sulfide Mineralized Bathtub Intrusion of the Duluth Complex, NE Minnesota, USA. *J. Petrol.* **2018**, *59*, 1167–1192.
7. Pan, L.-C.; Hu, R.-Z.; Wang, X.-S.; Bi, X.-W.; Zhu, J.-J.; Li, C. Apatite Trace Element and Halogen Compositions as Petrogenetic-Metallogenic Indicators: Examples from Four Granite Plutons in the Sanjiang Region, SW China. *Lithos* **2016**, *254*, 118–130.
8. O'Sullivan, G.; Chew, D.; Kenny, G.; Henrichs, I.; Mulligan, D. The Trace Element Composition of Apatite and Its Application to Detrital Provenance Studies. *Earth-Science Rev.* **2020**, *201*, 103044.
9. Mao, M.; Rukhlov, A.S.; Rowins, S.M.; Spence, J.; Coogan, L.A. Apatite Trace Element Compositions: A Robust New Tool for Mineral Exploration. *Econ. Geol.* **2016**, *111*, 1187–1222.
10. Ladenburger, S.; Marks, M.A.W.; Upton, B.; Hill, P.; Wenzel, T.; Markl, G. Compositional Variation of Apatite from Rift-Related Alkaline Igneous Rocks of the Gardar Province, South Greenland. *Am. Mineral.* **2016**, *101*, 612–626.
11. Krneta, S.; Cook, N.J.; Ciobanu, C.L.; Ehrig, K.; Kontonikas-Charos, A. The Wirrda Well and Acropolis Prospects, Gawler Craton, South Australia: Insights into Evolving Fluid Conditions through Apatite Chemistry. *J. Geochemical Explor.* **2017**, *181*, 276–291.
12. Cawthorn, R.G. Formation of Chlor-and Fluor-Apatite in Layered Intrusions. *Mineral. Mag.* **1994**, *58*, 299–306.
13. Belousova, E.A.; Griffin, W.L.; O'Reilly, S.Y.; Fisher, N.I. Apatite as an Indicator Mineral for Mineral Exploration: Trace-Element Compositions and Their Relationship to Host Rock Type. *J. Geochemical Explor.* **2002**, *76*, 45–69.
14. Holodnov, V.V.; Salihov, D.N.; Shagalov, E.S.; Konovalova, E.V.; Rahimov, I.R. The Role of Halogens and Sulfur in Apatite for Evaluation of Cu-Ni, Fe-Ti and Au Ores in Late Paleozoic Gabbroids of the West Magnitogorsk Zone (South Urals). *Mineralogia* **2015**, 45–61.
15. Barkov, A.Y.; Nikulin, I.I.; Nikiforov, A.A.; Lobastov, B.M.; Silyanov, S.A.; Martin, R.F. Atypical Mineralization Involving Pd-Pt, Au-Ag, REE, Y, Zr, Th, U, and Cl-F in the Oktyabrsky Deposit, Norilsk Complex, Russia. *Miner. 2021, Vol. 11, Page 1193* **2021**, *11*, 1193, doi:10.3390/MIN11111193.
16. Liu, M.-Y.; Zhou, M.-F.; Su, S.-G.; Chen, X.-G. Contrasting Geochemistry of Apatite from Peridotites and Sulfide Ores of the Jinchuan Ni-Cu Sulfide Deposit, NW China. *Econ. Geol.* **2021**, *116*, 1073–1092.
17. Sluzhenikin, S.F.; Yudovskaya, M.A.; Barnes, S.J.; Abramova, V.D.; Le Vaillant, M.; Petrenko, D.B.; Grigor'eva, A. V; Brovchenko, V.D. Low-Sulfide Platinum Group Element Ores of the Norilsk-Talnakh Camp. *Econ. Geol.* **2020**, *115*, 1267–1303, doi:10.5382/econgeo.4749.
18. Ryabov, V. V; Simonov, O.N.; Snisar, S.G. Fluorine and Chlorine in Apatites, Micas, and Amphiboles of Layered Trap Intrusions of the Siberian Platform. *Russ. Geol. Geophys.* **2018**, *59*, 363–373, doi:https://doi.org/10.1016/j.rgg.2017.05.003.
19. Rakhimov, I.R.; Gottman, I.A.; Kholodnov, V. V; Chervyakovskiy, V.S. Geochemistry of Accessory Apatite from the Cu–Ni–Sulfide-Bearing Ultramafic–Mafic Rocks of the Khudolaz Complex (South Urals) as a

Monitor of Magmatic and Metasomatic Processes. *Russ. Geol. Geophys.* **2022**, *63*, 1388–1406, doi:10.2113/RGG20214423.
20. Webster, J.D.; Sintoni, M.F.; De Vivo, B. The Partitioning Behavior of Cl, S, and H2O in Aqueous Vapor-±saline-Liquid Saturated Phonolitic and Trachytic Melts at 200 MPa. *Chem. Geol.* **2009**, *263*, 19–36, doi:https://doi.org/10.1016/j.chemgeo.2008.10.017.
21. Serova, A.A.; Spiridonov, E.M. Three Types of Apatite in Norilsk Sulfide Ores. *Geochemistry Int.* **2018**, *56*, 474–483, doi:10.1134/S0016702918050075.
22. Claiborne, L.L.; Miller, C.F.; Walker, B. a.; Wooden, J.L.; Mazdab, F.K.; Bea, F. Tracking Magmatic Processes through Zr/Hf Ratios in Rocks and Hf and Ti Zoning in Zircons: An Example from the Spirit Mountain Batholith, Nevada. *Mineral. Mag.* **2006**, *70*, 517–543, doi:10.1180/0026461067050348.
23. Watson, E.B.; Green, T.H. Apatite/Liquid Partition Coefficients for the Rare Earth Elements and Strontium. *Earth Planet. Sci. Lett.* **1981**, *56*, 405–421, doi:https://doi.org/10.1016/0012-821X(81)90144-8.
24. Warner, S.; Martin, R.F.; Abdel-Rahman, A.-F.M.; Doig, R. Apatite as a Monitor of Fractionation, Degassing, and Metamorphism in the Sudbury Igneous Complex, Ontario. *Can. Mineral.* **1998**, *36*, 981–999.
25. Järvinen, V.; Halkoaho, T.; Konnunaho, J.; Heinonen, J.S.; Rämö, O.T. Parental Magma, Magmatic Stratigraphy, and Reef-Type PGE Enrichment of the 2.44-Ga Mafic-Ultramafic Näränkävaara Layered Intrusion, Northern Finland. *Miner. Depos.* **2020**, *55*, 1535–1560, doi:10.1007/s00126-019-00934-z.
26. Halkoaho, T.A.A.; Alapieti, T.T.; Lahtinen, J.J.; Lerssi, J.M. The Ala-Penikka PGE Reefs in the Penikat Layered Intrusion, Northern Finland. *Mineral. Petrol.* **1990**, *42*, 23–38.
27. Groshev, N.Y.; Rundkvist, T. V; Karykowski, B.T.; Maier, W.D.; Korchagin, A.U.; Ivanov, A.N.; Junge, M. Low-Sulfide Platinum-Palladium Deposits of the Paleoproterozoic Fedorova-Pana Layered Complex, Kola Region, Russia. *Minerals* **2019**, *9*, 764.
28. Mitrofanov, F.P.; Bayanova, T.B.; Korchagin, A.U.; Groshev, N.Y.; Malitch, K.N.; Zhirov, D. V.; Mitrofanov, A.F. East Scandinavian and Noril'sk Plume Mafic Large Igneous Provinces of Pd-Pt Ores: Geological and Metallogenic Comparison. *Geol. Ore Depos.* **2013**, *55*, 305–319, doi:10.1134/S107570151305005X.
29. Alapieti, T.T.; Filén, B.A.; Lahtinen, J.J.; Lavrov, M.M.; Smolkin, V.F.; Voitsekhovsky, S.N. Early Proterozoic Layered Intrusions in the Northeastern Part of the Fennoscandian Shield. *Mineral. Petrol.* **1990**, *42*, 1–22, doi:10.1007/BF01162681.
30. Maier, W.D.; Halkoaho, T.; Huhma, H.; Hanski, E.; Barnes, S.-J. The Penikat Intrusion, Finland: Geochemistry, Geochronology, and Origin of Platinum–Palladium Reefs. *J. Petrol.* **2018**, *59*, 967–1006, doi:10.1093/petrology/egy051.
31. Iljina, M. The Portimo Layered Igneous Complex: With Emphasis on Diverse Sulphide and Platinum-Group Element Deposits. Ph.D. Thesis, University of Oulu, Oulu, Finland, 1994; 158 p.
32. Karykowski, B.T.; Maier, W.D.; Groshev, N.Y.; Barnes, S.J.; Pripachkin, P. V.; McDonald, I.; Savard, D. Critical Controls on the Formation of Contact-Style PGE-Ni-Cu Mineralization: Evidence from the Paleoproterozoic Monchegorsk Complex, Kola Region, Russia. *Econ. Geol.* **2018**, *113*, 911–935, doi:10.5382/econgeo.2018.4576.
33. Chashchin, V. V.; Mitrofanov, F.P. The Paleoproterozoic Imandra-Varzuga Rifting Structure (Kola Peninsula): Intrusive Magmatism and Minerageny. *Geodin. i Tektonofiz.* **2015**, *5*, 231–256.
34. Fedorova Tundra is Europe's Largest Deposit of Platinum Group Metals. Available online: https://fedorovoresources.ru/en/#field (accessed on 31/10/2023)
35. What – Suhanko – Arctic Platinum Oy. Available online: https://www.suhanko.com/what (accessed on 31/10/2023)
36. Subbotin, V. V; Vymazalová, A.; Laufek, F.; Savchenko, Y.E.; Stanley, C.J.; Gabov, D.A.; Plášil, J. Mitrofanovite, Pt 3 Te 4, a New Mineral from the East Chuarvy Deposit, Fedorovo--Pana Intrusion, Kola Peninsula, Russia. *Mineral. Mag.* **2019**, *83*, 523–530.
37. Vymazalová, A.; Subbotin, V. V.; Laufek, F.; Savchenko, Y.E.; Stanley, C.J.; Gabov, D.A.; Plášil, J. Panskyite, Pd 9 Ag 2 Pb 2 S 4 , a New Platinum Group Mineral from the Southern Kievey Ore Occurrence of the Fedorova–Pana Layered Intrusion, Kola Peninsula, Russia . *Mineral. Mag.* **2020**, 1–11, doi:10.1180/mgm.2020.100.
38. Groshev, N.Y.; Rundqvist, T.V.; Mansur, E.T.; Barnes, S.-J.; Ivanov, A.N. Sushchenko, A.M. Geochemical and Geochronological Evidence of an Unusual Sequence of Formation of the West Pana Layered Intrusion. In Proceedings of the Ultramafic-mafic complexes: geology, structure, ore potential; 2022; pp. 34–37.
39. Pripachkin, P.; Rundkvist, T.; Groshev, N. Paleoproterozoic East Pana Layered Intrusion (Kola Peninsula, Russia): Geological Structure, Petrography, Geochemistry and Cu-Ni-PGE Mineralization. *Minerals* **2023**, *13*, 681.
40. Schissel, D.; Tsvetkov, A.A.; Mitrofanov, F.P.; Korchagin, A.U. Basal Platinum-Group Element Mineralization in the Federov Pansky Layered Mafic Intrusion, Kola Peninsula, Russia. *Econ. Geol.* **2002**, *97*, 1657–1677, doi:10.2113/gsecongeo.97.8.1657.

41. Korchagin, A.U.; Goncharov, Y. V.; Subbotin, V. V.; Groshev, N.Y.; Gabov, D.A.; Ivanov, A.N.; Savchenko, Y.E. Geology and Composition of the Ores of the Low-Sulfide North Kamennik PGE Deposit in the West-Pana Intrusion. *Ores Met.* **2016**, *1*, 42–51.
42. Korchagin, A.U.; Subbotin, V. V; Mitrofanov, F.P.; Mineev, S.D. Kievey PGE-Bearing Deposit in the West-Pana Layered Intrusion. In Strategic Mineral Resources of Lapland; Mitrofanov, F., et al., Ed.; Geological institute KSC RAS: Apatity 2009, pp. 12–32.
43. Kalinin, A.A. Precious Metal Mineralization in the East Pansky Layered Massif. In Proceedings of the The Fennoscandian School of Ore Genesis in Layered Intrusions; Groshev, N.Y., Ed.; Geological institute KSC RAS: Apatity, 2021; pp. 20–23.
44. Groshev, N.; Karykowski, B. The Main Anorthosite Layer of the West-Pana Intrusion, Kola Region: Geology and U-Pb Age Dating. *Minerals* **2019**, *9*, 71, doi:10.3390/min9020071.
45. Latypov, R.M.; Mitrofanov, F.P.; Alapieti, T.T.; Halkoaho, T.A.A. Petrology of the Lower Layered Horizon of the Western Pansky Tundra Intrusion, Kola Peninsula. *Petrology* **1999**, *7*, 482–508.
46. Latypov, R.M.; Mitrofanov, F.P.; Skiba, V.I.; Alapieti, T.T. The Western Pansky Tundra Layered Intrusion, Kola Peninsula: Differentiation Mechanism and Solidification Sequence. *Petrology* **2001**, *9*, 214–251.
47. Groshev, N.Y.; Ivanov, A.N.; Huber, M. PGE Reefs of the West-Pana Layered Intrusion, Kola Region, Russia: Plagioclase Composition as an Indicator of the Economic Potential. In Proceedings of the IOP Conference Series: Earth and Environmental Science; 2019; Vol. 302, p. 12041.
48. Groshev, N.Y.; Rundkvist, T.V.; Korchagin, A.U.; Ivanov, A.N. Concentrations of Trace Elements in Rocks of the Lower Layered Horizon of the West-Pana Intrusion. In Proceedings of the 12th International Platinum Symposium, 11 – 14 August 2014, Yekaterinburg, Russia; 2014; pp. 65–66.
49. Bayanova, T.B. Age of Reference Geological Complexes of the Kola Region and Duration of Magmatic Processes; Nauka: St. Petersburg, 2004;
50. Korchagin, A.U. Report on the Results of Geological Exploration at the Kievey PGE Deposit, Feasibility Study of Temporary Exploration Conditions and Calculation of Platinum Group Metals, Copper and Nickel Reserves; TFGI: Apatity, Russia, 2007;
51. Nikulin, I.I.; Mikhailova, Y.A.; Kalashnikov, A.O. Groshev, N.Yu. Stepenshchikov, D.G. Pakhomovskiy, Ya.A. Kadyrov, R.I. *Structural, Textural and Material Properties of Sulfide Copper-Nickel Ores*; 2022;
52. Minerals-Concentrators of d- and f-Elements: Local Spectroscopic and LA-ICP-MS Studies of Composition, Structure and Properties, Geochronological Applications; Votyakov, S.L., Ed.; Publishing House SB RAS: Novosibirsk, 2020;
53. Dudkin, K.O.; Rundkvist, T.V. Brown Plagioclases as a Source of Magnetic Anomalies of the Pana Massif. *Russ. Geophys. J.* **2002**, *27*, 25–35.
54. Warr, L.N. IMA--CNMNC Approved Mineral Symbols. *Mineral. Mag.* **2021**, *85*, 291–320.
55. O'Shea, D.C.; Bartlett, M.L.; Young, R.A. Compositional Analysis of Apatites with Laser-Raman Spectroscopy: (OH,F,Cl)Apatites. *Arch. Oral Biol.* **1974**, *19*, 995–1006, doi:https://doi.org/10.1016/0003-9969(74)90086-7.
56. Penel, G.; Leroy, G.; Rey, C.; Bres, E. MicroRaman Spectral Study of the PO4 and CO3 Vibrational Modes in Synthetic and Biological Apatites. *Calcif. Tissue Int.* **1998**, *63*, 475–481, doi:10.1007/s002239900561.
57. Antonakos, A.; Liarokapis, E.; Leventouri, T. Micro-Raman and FTIR Studies of Synthetic and Natural Apatites. *Biomaterials* **2007**, *28*, 3043–3054, doi:https://doi.org/10.1016/j.biomaterials.2007.02.028.
58. Awonusi, A.; Morris, M.D.; Tecklenburg, M.M.J. Carbonate Assignment and Calibration in the Raman Spectrum of Apatite. *Calcif. Tissue Int.* **2007**, *81*, 46–52, doi:10.1007/s00223-007-9034-0.
59. Rey, C.; Marsan, O.; Combes, C.; Drouet, C.; Grossin, D.; Sarda, S. Characterization of Calcium Phosphates Using Vibrational Spectroscopies. In *Advances in Calcium Phosphate Biomaterials*; Ben-Nissan, B., Ed.; Springer Berlin Heidelberg: Berlin, Heidelberg, 2014; pp. 229–266 ISBN 978-3-642-53980-0.
60. Fau, A.; Beyssac, O.; Gauthier, M.; Panczer, G.; Gasnault, O.; Meslin, P.-Y.; Bernard, S.; Maurice, S.; Forni, O.; Boulliard, J.-C.; et al. Time-Resolved Raman and Luminescence Spectroscopy of Synthetic REE-Doped Hydroxylapatites and Natural Apatites. *Am. Mineral.* **2022**, *107*, 1341–1352, doi:10.2138/am-2022-8006.
61. Groshev, N.Y.; Nikulin, I.I.; Sushchenko, A.M.; Mikhailova, Y.A.; Kalashnikov, A.O.; Pakhomovsky, Y.A.; Kadyrov, R.I. Composition of Apatite from Picritic Gabbro-Dolerites of the Kharaelakh Intrusion: First Systematic Data along the Section. *Tr. FNS* **2023**, 68–76.
62. Latypov, R.M. Lower Layered Horizon of the Pana Tundra Intrusion: Structure, Ore Potential, Petrogenesis. Ph.D. Thesis, IGGP RAS, St.-Petersburg, Russia, 1995; 123 p.
63. McDonough, W.F.; Sun, S.-S. The Composition of the Earth. *Chem. Geol.* **1995**, *120*, 223–253.
64. Boudreau, A.E.; Kruger, F.J. Variation in the Composition of Apatite through the Merensky Cyclic Unit in the Western Bushveld Complex. *Econ. Geol.* **1990**, *85*, 737–745.
65. Barnes, S.J.; Malitch, K.N.; Yudovskaya, M.A. Introduction to a Special Issue on the Norilsk-Talnakh Ni-Cu-Platinum Group Element Deposits. *Econ. Geol.* **2020**, *115*, 1157–1172, doi:10.5382/econgeo.4750.
66. Voloshina, Z.M.; Petrov, V.P.; Popova, L.I.; Rezhenova, S.A. Metamorphic Parageneses in Rocks of the Lower Layered Horizon of the Pana Tundra Intrusion (Kola Peninsula). *Zap. RMO* **1998**, *3*, 57–65.

67. Karzhavin, V.K.; Voloshina, Z.M. Simulation of Metamorphism and Fluid Regime in the Mineralized Unit of the Pana Massif in Relation to Its PGE Ore Mineralization. *Geochemistry Int.* **2006**, *44*, 475–484.
68. Voloshina, Z.M.; Karzhavin, V.K.; Petrov, V.P. Metamorphism and Ore Genesis in the Platinum-Bearing Pana Intrusive Massif (Kola Peninsula); Publishing house KSC RAS: Apatity, 2008;
69. Subbotin, V. V.; Korchagin, A.U.; Savchenko, E.E.; others Platinum Mineralization of the Fedorova-Pana Ore Node: Types of Ores, Mineral Compositions and Genetic Features. *Vestn. Kola Sci. Cent. Russ. Acad. Sci. Apatity* **2012**, *1*, 54–65.
70. Nivin, V.A.; Rundqvist, T. V Formation of Pt-Bearing Western Pana Pluton on the Kola Peninsula: Fluid Regime as Deduced from Helium and Argon Isotopic Compositions. *Geol. Ore Depos.* **2017**, *59*, 36–55.
71. Campbell, I.; Naldrett, A.; Barnes, S. A Model for the Origin of the Platinum-Rich Sulfide Horizons in the Bushveld and Stillwater Complexes. *J. Petrol.* **1983**, *24*, 133–165, doi:10.1093/petrology/24.2.133.
72. Naldrett, A.J.; Gasparrini, E.C.; Barnes, S.J.; Von Gruenewaldt, G.; Sharpe, M.R. The Upper Critical Zone of the Bushveld Complex and the Origin of Merensky-Type Ores. *Econ. Geol.* **1986**, *81*, 1105–1117.
73. Ivanov, A.N.; Chernyavsky, A. V; Groshev, N.Y.; Savchenko, E.E. PGM Assemblages from the Lower Ore Bodies of the North Kamennik Palladium Deposit, Kola Region, Russia. In Proceedings of the IOP Conference Series: Earth and Environmental Science; 2020; Vol. 539, p. 12151.
74. Barnes, S.J.; Fiorentini, M.L.; Austin, P.; Gessner, K.; Hough, R.M.; Squelch, A.P. Three-Dimensional Morphology of Magmatic Sulfides Sheds Light on Ore Formation and Sulfide Melt Migration. *Geology* **2008**, *36*, 655–658.